Journal of Petroleum Exploration and Production Technology (2023) 13:1655–1667
https://doi.org/10.1007/s13202-023-01633-2

ORIGINAL PAPER-PRODUCTION ENGINEERING

Improving reservoir permeability by electric pulse controllable shock wave

Xinguang Zhu[1] · Chun Feng[1] · Pengda Cheng[1]

Received: 27 September 2022 / Accepted: 11 April 2023 / Published online: 28 April 2023

Abstract

Controllable shock wave (CWS) parameters such as amplitude, operating area and number of operations are easy to control and have received extensive attention as a potential new technology for reservoir permeability enhancement. Based on the continuous-discontinuous element method (CDEM) and considering the coupling mechanism of reservoir deformation, failure, pore seepage and fracture flow, a multiphysical field coupling model of reservoir permeability enhancement under CWS is proposed. Under the fluid–solid coupling condition, the formation and development dynamic process of reservoir fractures are obtained, and the change of reservoir permeability is also obtained. The compression fracture zone, tensile fracture zone and undamaged zone are formed around the wellbore. After repeated impact, the number of fractures is more sensitive to tectonic stress, the fracture aperture is more sensitive to reservoir strength. Different from hydraulic fracturing, a large number of fractures in different directions will appear around the main fracture after repeated impact, forming a complex fracture network similar to spider web, which may be beneficial to improve reservoir permeability. The permeability of reservoirs with different tectonic stresses and strengths increases nonlinearly and monotonicly with repeated impacts. Based on CDEM, the change of reservoir permeability with tectonic stress, strength and impact times is obtained, which is a nonlinear monotonic three-dimensional relationship. Based on that relationship, the parameters of CWS can be controlled to predict the change of reservoir permeability, such as peak pressure, duration, impact times, etc. Therefore, it can optimize the reservoir fracturing scheme and improve the reservoir fracturing efficiency, which has considerable practical significance in engineering.

Keywords Controllable shock wave · continuous-discontinuous element method · Coupling model · Fracture · Reservoir permeability

Abbreviations

CDEM	Continuous-discontinuous element method
CRI	Cuttings reinjection
CWS	Controllable shock wave
DDM	Displacement discontinuity method
FEM	Finite element method
ILSA	Implicit level set algorithm
PWRI	Produced water reinjection
XFEM	Extended finite element method

Latin letters

$\boldsymbol{a}_{\mathrm{n}}$	Nodal acceleration (ms^{-2})
$\boldsymbol{B}_i$	Strain matrix in Gaussian point i (-)
$[\boldsymbol{C}]$	Damping matrix (-)
E	Young's modulus (GPa)
$\boldsymbol{F}$	Force (N)
$\boldsymbol{J}_i$	Jacobi determinant in Gaussian point i (-)
M_{T}	Total mass of water injection (kg)
$[\boldsymbol{M}]$	Mass matrix (-)
$[\boldsymbol{K}]$	Stiffness matrix (-)
T	Impact times (-)
$\boldsymbol{u}_{\mathrm{n}}$	Nodal displacement (m)
$\boldsymbol{v}_{\mathrm{n}}$	Nodal velocity (ms^{-1})
w	Fracture aperture (m)
w_i	Integral coefficient in Gaussian point i (-)

Greek letters

α	Biot coefficient (-)
$\boldsymbol{\sigma}_i$	Stress in Gaussian point i (Pa)
$\boldsymbol{\sigma}_{\mathrm{ini}}$	Tectonic stress (MPa)
$\boldsymbol{\varepsilon}_i$	Strain in Gaussian point i (-)
κ	Permeability ratio (m^2)

✉ Pengda Cheng
pdcheng@imech.ac.cn

[1] Key Laboratory for Mechanics in Fluid Solid Coupling Systems, Institute of Mechanics, Chinese Academy of Sciences, Beijing 100190, China

κ_0	Initial permeability ratio (m^2)
κ^F	Permeability of fracture seepage ($m^2Pa^{-1}\ s^{-1}$)
μ	Fluid dynamic viscosity (Pa·s)
φ	Porosity %
φ_0	Initial porosity %
Φ	Fracture degree %

Introduction

Fracturing technology is an important technology in petroleum engineering and plays a critical role in many applications within the oil and natural gas industry. The process can be generally considered as the intentional (or unintentional) initiation and propagation of a fracture due to the pressurization of fluid that flows within the fracture (Shi et al. 2023). Examples of applications include (a) the stimulation of rock formations with poor or damaged permeability to increase conductivity between the reservoir and the producing wells, (b) improvement of produced water reinjection (PWRI) where water is injected to replace produced fluids and maintain reservoir pressure or provide enhanced oil recovery, (c) cuttings reinjection (CRI) where a slurry of drill cuttings is injected into a formation to mitigate the cost and risk of surface disposal, (d) in situ stress measurement by balancing the fracturing fluid pressure in a hydraulically opened fracture with the geostatic stresses, and (e) wellbore integrity analysis of drilling operations to avoid propagating near-wellbore fractures that could result in drilling fluid losses to the formation and an inability to effectively clean the wellbore. Hydraulic fracturing and deflagration fracturing are commonly used in engineering. Hydraulic fracturing has improved energy production significantly in past decades (Chen et al. 2022). Offshore hydraulic fracturing may be limited by objective conditions, such as small offshore platform space and thin reservoir near water, which leads to challenges in reservoir stimulation (Azad et al. 2022). Parvizi et al. (2017) proposed a practical workflow for offshore hydraulic fracturing modeling, focusing on the North Sea and extending it to offshore oil fields in the Persian Gulf. Deflagration fracturing is a reservoir stimulation technology that has been applied in energy production in recent years (Wu et al. 2018a; Yu et al. 2022). Gong et al. (2022) has developed a new stimulation technology, which is based on deflagration fracturing of radial wells and uses explosives to increase reservoir production. Deflagration fracturing has a good stimulation effect, but it involves explosives or solid propellant (solid rocket fuel), which has potential safety hazards. Therefore, offshore oil platforms need a new reservoir reconstruction technology with high efficiency, safety and low cost. CSW fracturing is a new technology developed in this field in recent years (Wu et al. 2018b; Qin et al. 2021; Wang et al. 2021). The CSW adopts an electric explosion of metal wire, which can produce a strong shock wave propagating outward in water. Unlike explosives and hydraulic fracturing, explosives produce supersonic shock waves in a very short time, while hydraulic fracturing produces pressure pulses in a long time. The time of shock wave of CSW is between explosive and hydraulic fracturing. The amplitude, impulse, action area and operation times of the CSW are easy to control, which can realize single point multiple impact or multipoint continuous impact on the reservoir. In recent years, CSW fracturing technology has been successfully applied to improve the permeability of coal seams, and the application of CWS in offshore reservoirs has been explored (Qin et al. 2021). Based on the experiment, CWS can effectively change the internal structure of rock, and then change the compressive strength and tensile strength of the reservoir (Zhang et al. 2016; Yang et al. 2020).

Due to the limitations of experiment and monitoring, the mechanism of rock fracture caused by CWS has not been fully understood. Therefore, numerical methods are used to simulate the dynamic process of rock fracture and analyze the rock fracture mechanism, which has also received extensive attention. For the evaluation of fracturing technology to increase reservoir permeability since the 1980s, many simplified hydraulic fracturing formulas have been used in the oil and natural gas industry for the rapid design, analysis and prediction of fracture size, treating pressures, and flows. These methods rely on strong simplified assumptions so that some problems can be solved in reality. Their reliability and accuracy are restricted to unrealistic scenarios that apply intrinsic simplistic assumptions, i.e., situations where some of the coupling between the many different processes involved can be neglected and with strong symmetry in confinement stresses and geology. The accurate modeling of the fracturing process under realistic geologies, wellbore configurations, confining stress states, and operational conditions calls for a more advanced, multiphysics numerical method that incorporates the complex coupling between the injected fluid, the pore fluid, the rock deformation, and the fracture configuration. As a result, more accurate numerical methods have been used to simulate fracturing problems since the 2000s. Typical examples of fluid–solid coupled seepage numerical methods based on continuum mechanics include the displacement discontinuity method (DDM) (Peirce et al. 2001), finite element method (FEM) (Lecampion et al. 2018; Ma et al. 2021; Shen et al. 2022), extended finite element method (XFEM) (Li et al. 2018; Maulianda et al. 2020; Zhang et al. 2020; Esfandiari et al. 2023) and implicit level set algorithm (ILSA) (Dontsov et al. 2017). For the finite element method, the mesh must be in accordance with the boundary of the cracks, which will require constant remeshing to trace the crack propagation. The mapping of physical information between the old and new meshes after remeshing will lead to a decrease in computational accuracy.

Although the XFEM can avoid remeshing, it requires a very fine mesh in the solution domain, which consumes considerable computing time when the crack path is unknown in advance. As a result, it is difficult to simulate the complex propagation and intersection of multiple cracks using XFEM.

CSW fracturing has received extensive attention as a potential new technology for reservoir permeability enhancement. Under the action of shock waves, the rock fracturing process is very complex, and it is a dynamic process involving the multiphysics coupling of solid deformation, failure, pore seepage and fracture flow. At present, the research focuses on theoretical analysis and experimental measurement, and the mechanism of rock fracturing under the coupling of multiple physical fields still needs further research. Therefore, there is a significant necessity to understand the coupling behavior of geomechanics and fluid flow under shock waves to optimize extraction conditions and enhance reservoir permeability. Based on the CDEM, the coupling mechanism of deformation, failure, pore seepage, and fracture flow is considered, and a multiphysical field coupling model for reservoir permeability enhancement under CWS is proposed and validated. Under the fluid–solid coupling condition, the formation and development dynamic process of reservoir fractures are obtained, and the change of reservoir permeability is also obtained. Different from hydraulic fracturing, a large number of fractures in different directions will appear around the main fracture after repeated impact, forming a complex fracture network similar to spider web, which may be beneficial to improve reservoir permeability.

Coupled numerical model of CSW fracturing

The computational modeling of CSW fracturing of rock is a challenging endeavor. The difficulty originates primarily from the strong nonlinear coupling between the governing equations, as the process involves at least the interaction between four different phenomena: (i) the flow of the fracturing fluid within the fracture, (ii) the flow of the pore fluid and seepage of fracturing fluid within the pores, (iii) the deformation of a porous medium induced by both the hydraulic pressurization of the fracture and the compression/expansion and transport of pore fluid within the pores, and (iv) fracture propagation, which is an inherently irreversible and singular process. Additionally, fracture propagation typically occurs in heterogeneous formations consisting of multiple layers of different rock types subjected to in situ confining stresses with nonuniform magnitudes and orientations. Therefore, it is very important to consider the coupling model of reservoir deformation, fracture, pore seepage and fracture flow to evaluate the fracturing effect of CSW.

Rock deformation and failure models

The rock deformation and failure model are based on the continuous-discontinuous element method. CDEM is an explicit numerical analysis method based on the Lagrange equation, which is mainly used to simulate the progressive failure process of materials, and has been widely used in recent years (Yue et al. 2021; Zhu et al. 2021; Feng et al. 2022; Li et al. 2022; Wang et al. 2022). The calculation domain of CDEM usually includes continuous blocks and discrete blocks, which are used as the calculation domain of finite element method and discrete element method, respectively. The blocks are composed of one or more continuous elements, which are used to describe the continuous properties of materials, such as elasticity and plasticity. The common boundary between blocks is the interface, which is used to describe the discontinuous properties of materials such as fracture, slip and collision.

The governing equations can be expressed as a system of equilibrium equations in the following matrix form:

$$[\boldsymbol{M}]\boldsymbol{u}'' + [\boldsymbol{C}]\boldsymbol{u}' + [\boldsymbol{K}]\boldsymbol{u} = \boldsymbol{F} \tag{1}$$

where $[\boldsymbol{M}]$, $[\boldsymbol{C}]$, and $[\boldsymbol{K}]$ are the mass matrix, damping matrix, and stiffness matrix, respectively, $\boldsymbol{u}$ represents the element displacement vector, and $\boldsymbol{F}$ is the external force vector, including the solid force and fluid pressure.

The main steps to calculate the node force by the strain matrix with the incremental method are written as

$$\begin{cases} \Delta\boldsymbol{\varepsilon}_i = \boldsymbol{B}_i \Delta\boldsymbol{u}_e \\ \Delta\boldsymbol{\sigma}_i = \boldsymbol{D}\Delta\boldsymbol{\varepsilon}_i \\ \boldsymbol{\sigma}_i^n = \boldsymbol{\sigma}_i^{n-1} + \Delta\boldsymbol{\sigma}_i \\ \boldsymbol{F}_e = \sum_{i=1}^{N} \boldsymbol{B}_i^T \boldsymbol{\sigma}_i^n w_i \boldsymbol{J}_i \end{cases} \tag{2}$$

where $\boldsymbol{B}_\mathrm{i}$, $\Delta\boldsymbol{\varepsilon}_\mathrm{i}$, $\Delta\boldsymbol{\sigma}_\mathrm{i}$, w_i, $\boldsymbol{J}_\mathrm{i}$ are the strain matrix, incremental strain, incremental stress, integral coefficient, and Jacobi determinant in Gaussian point i, respectively; n and n-1 represent the current and previous moments in Gaussian point i, respectively; $\boldsymbol{D}$, $\Delta\boldsymbol{u}_\mathrm{e}$, $\boldsymbol{F}_\mathrm{e}$ are the elastic matrix, incremental displacement vector and node force vector of element, respectively; N is the total number of Gaussian points.

Euler's forward difference method is used for explicit iterative solution, and the nodal velocity and nodal acceleration of the elements can be calculated through the time-stepping scheme as follows:

$$\begin{cases} \boldsymbol{v}_n = \dfrac{\boldsymbol{u}_{n+1} - \boldsymbol{u}_n}{\Delta t} \\ \boldsymbol{a}_n = \dfrac{\boldsymbol{u}_{n+1} - 2\boldsymbol{u}_n + \boldsymbol{u}_{n-1}}{(\Delta t)^2} \end{cases} \tag{3}$$

where $\boldsymbol{u}$n is nodal displacement of the elements, $\boldsymbol{v}_{\mathrm{n}}$ is nodal velocity of the elements, $\mathbf{a}$n is nodal velocity of the elements.

The interaction between these discrete blocks can be transformed into virtual spring forces. The forces at the contact interface of two blocks in the local coordinate can be expressed as:

$$\boldsymbol{F}_{nt} = -K_{nt} \times \Delta \boldsymbol{u}_{nt} \tag{4}$$

$$\boldsymbol{F}_{s} = -K_{s} \times \Delta \boldsymbol{u}_{s} \tag{5}$$

where $\boldsymbol{F}$, K, and $\Delta \boldsymbol{u}$ are the incremental force, stiffness, and relative displacement of the virtual spring, respectively, and nt and s represent the normal and tangential directions, respectively.

When a given failure criterion of the virtual springs is reached, the connected interface between the blocks is transformed into a discontinuous fracture surface. In this paper, the tensile strength is governed by the maximum tensile stress criterion, and the shear strength is described by the Mohr−Coulomb model.

Pore seepage and fracture flow models

For pore seepage, the reservoir rock deformation caused by pressure causes considerable changes in porosity and permeability. The porosity and permeability models of pore seepage considering the reservoir rock deformation can be expressed as (Cheng et al. 2022),

$$\varphi = \alpha + (\varphi_0 - \alpha) \exp\left(-\frac{\Delta \sigma'}{K}\right) \tag{6}$$

$$\frac{\kappa}{\kappa_0} = \left(\frac{\varphi}{\varphi_0}\right)^3 \tag{7}$$

where φ_0 and κ_0 are the initial porosity and the initial permeability, respectively; α is the Biot coefficient; and σ' is the effective mean stress.

For fracture flow, the permeability models can be expressed as

$$\kappa^F = \frac{w^2}{12\mu} \tag{8}$$

where κ^{F} is the permeability of fracture seepage; w is the fracture aperture, which is related to the node displacement after rock fracture; and μ is the fluid dynamic viscosity.

Model validation

In order to simulate hydraulic fracturing, this paper proposes a three-dimensional hydraulic fracturing model based on CDEM, which includes not only the fracture seepage of fluid flow in joints or fractures but also the pore seepage in the rock mass and the coupling between them. This model can also simulate the whole process of cracks from initiation and propagation to intersection driven by fluid. Through the relationship between fluid flow, medium saturation and fluid pressure, the coupling of pore seepage and fracture flow is realized. Through the effective stress principle, the coupling of solid deformation and pore seepage is realized. Through the relationship between fluid pressure, solid displacement and fracture aperture, the coupling of solid deformation and fracture flow is realized. Furthermore, by comparison with previous research results, the accuracy of the pore seepage and fracture flow models is verified (Yang et al. 2018; Zhu et al. 2021). Through the analytical solution of the Mandel-Cryer effect, the coupling model of solid deformation and pore seepage is verified (Cheng et al. 2016; Zhu et al. 2021). The effectiveness of the coupling model in calculating geometric shapes such as fracture aperture, fracture direction and distribution is verified by previous hydraulic fracturing research results (Tan et al. 2017; Dontsov et al. 2018; Zhu et al. 2021).

Improving reservoir permeability by CSW fracturing

Physical and mechanical parameters of CSW

Based on the experimental data (Zhang et al. 2016; Yang et al. 2020), the initial energy of the electric explosion system is 30 kJ, and the charging voltage is 24 kV. The peak pressure of the shock wave is greater than 100 MPa under water, and the period of the shock wave is approximately 500 ms. The pressure of typical CWS changes with time is shown in Fig. 1. Considering the relationship between the wave velocity in the rock and the size of the calculation domain, the time interval of the CSW is greater than 300 ms, and the pressure of CWS with 10 impacts changes with time is shown in Fig. 2.

Geometry for the CWS fracturing model

Wells in offshore oil fields usually adopt a combination of parameters, such as a perforation diameter of 10–40 mm, hole density of 10–40 holes/m, and phase angles of 45°, 60°, 90°, 120°, 135°, and 180° (Prasad Singh et al. 2019). When the perforation diameter is approximately 10 mm, the productivity is much lower than other perforation diameters, while when the perforation diameter is greater than 20 mm, the productivity increase is not obvious. In addition, when the perforation phase is 45° or 90°, the productivity is higher than that in other perforation phases. According to the optimized geometric parameters of offshore oil wells, the well

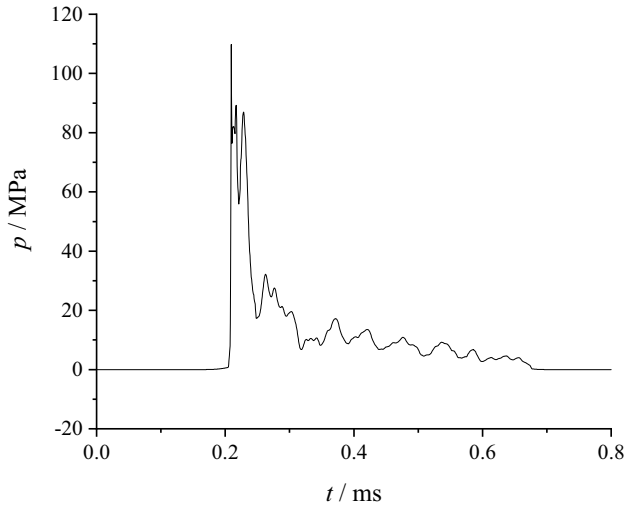

Fig. 1 Pressure of typical CWS change with time

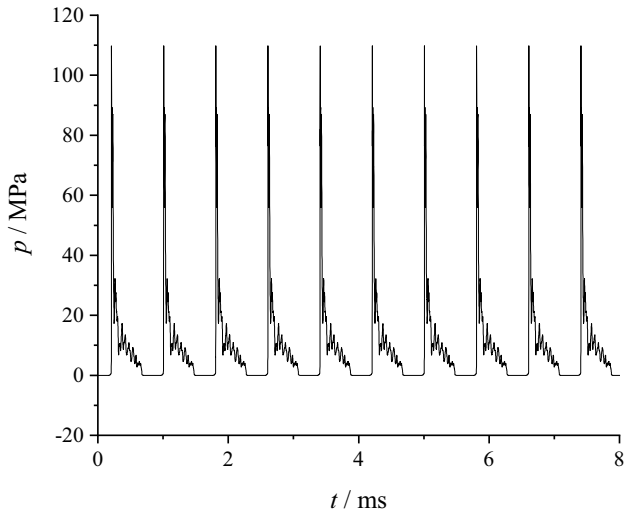

Fig. 2 Pressure of CWS with 10 impacts change with time

radius is 122.24 mm, the casing wall thickness is 11.99 mm, the perforation radius is 10 mm, and the perforation phase is 90°, as shown in Fig. 3. The rock radius of CWS fracturing is set to 1 m. In this paper, the fracture propagation along the perforation direction is mainly considered. After the sensitivity test of the mesh size, the minimum size of the mesh is set to 1 mm.

Material properties

In this paper, the physical and mechanical parameters of rock mainly refer to the Bohai Reservoir (Yang et al. 2020). The uniaxial compressive strength is 7.6 MPa to 56.1 MPa, The uniaxial tensile strength of reservoirs is 1.78 MPa to 3.22 MPa. For low-permeability reservoirs, the average

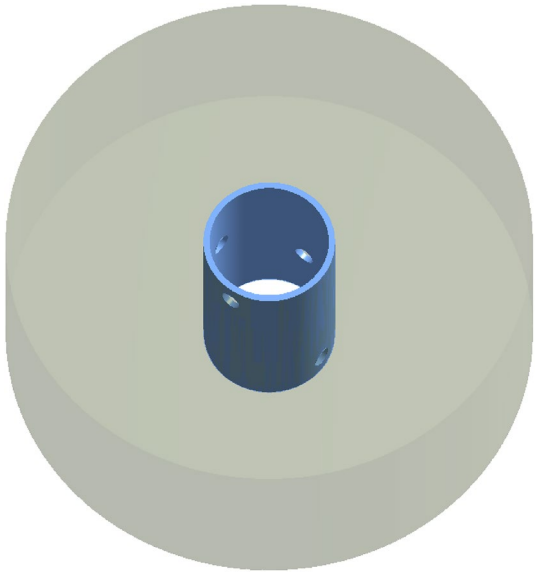

Fig. 3 Cylindrical domain with a horizontal, circular-shaped, CSW driven fracture

density of the conglomerate rocks is 2640 kg/m^3, the effective porosity is obtained from 6 to 20%, with an average of 12.4%, and the permeability is obtained from 0.8 mD to 50 mD, with an average of 12.5 mD. The detailed reservoir properties used in the simulation are listed in Table 1.

Three rocks of varying strength are selected. Based on the Mohr–Coulomb model, the mechanical parameters of the three rocks are shown in Table 2.

Initial conditions, boundary conditions and loads

In the calculation of CSW fracturing to improve reservoir permeability, the solid–fluid coupling effect is very obvious. The initial conditions and boundary conditions are set as follows.

Solid Field: The initial displacement is 0, and the initial stress refers to the tectonic stress. The inner wall of the casing is a normal displacement boundary condition, and the displacement value is 0. The outer surface of the rock is a normal pressure boundary condition, the pressure value is related to the tectonic stress, and a nonreflection boundary is set for the shock wave.

Fluid field: the initial flow velocities of pore seepage and fracture flow are both 0, and the initial flow field pressure refers to the tectonic stress. The perforation is the boundary condition of the flow pressure, and the pressure value refers to the time evolution of the CSW pressure for 10 shocks, as shown in Fig. 2. The outer surface of the rock is the boundary condition of flow pressure, and the pressure value is related to the tectonic stress.

Discussions

Effect of tectonic stress

The tectonic stress has a great influence on the formation and development of fractures. Under the tectonic stress conditions of 1 MPa, 3 MPa and 5 MPa, the influence of tectonic stress on reservoir permeability after repeated impact is analyzed. When the tectonic stress is 1 MPa and 5 MPa, the maximum principal stress of Rock1 after the 10th impact is shown in Fig. 4. The stress wave of CWS is transmitted to the reservoir along the perforation. At the same time, the propagation distance of the stress wave is similar in different tectonic stress reservoirs, and the maximum principal stress is also similar. For the range of tensile stress caused by repeated impact, reservoirs with low tectonic stress are much larger than reservoirs with high tectonic stress. The area near the wellbore is compressed by the CSW stress wave, and compressive fractures appear in the reservoir. Along the formation of the fracture, the pressure will transfer rapidly with the fracture flow. Under the effect of fluid pressure, tensile stress will be generated in the front of the fracture. When the tensile stress is greater than the tensile strength of reservoir, the tensile fractures appear far away from the wellbore in the reservoir. With the increase of the number and length of

Table 1 Physical and mechanical parameters of the low permeability reservoir

Parameters	Value	Parameters	Value
Rock density	2640 kg/m^3	Initial water density	998.2 kg/m^3
Elastic modulus	5–37 GPa	Water viscosity	1.01×10^{-3} Pa·s
Poisson's ratio	0.2–0.3	Bulk modulus of water	2.19 × 109 Pa
Cohesive force	2–30 MPa	Reservoir porosity	6%–20%
Interior friction angle	30°–45°	Reservoir permeability	12.5mD
Compression strength	7.6–56.1 MPa	Biot coefficient	0.4–0.8
Tensile strength	1–3.22 MPa	Initial water saturation	0.95
Initial tectonic stress	1–5 MPa		

Table 2 Rock mechanical parameters of the reservoir

	Elastic modulus/GPa	Poisson's ratio	Cohesive force/MPa	Friction angle/°	Tensile strength/MPa	Compression strength/MPa
Rock1	9.13	0.25	5.01	30	1.78	26.86
Rock2	22.71	0.23	8.72	37	2.51	37.65
Rock3	36.29	0.22	12.42	43	3.22	48.44

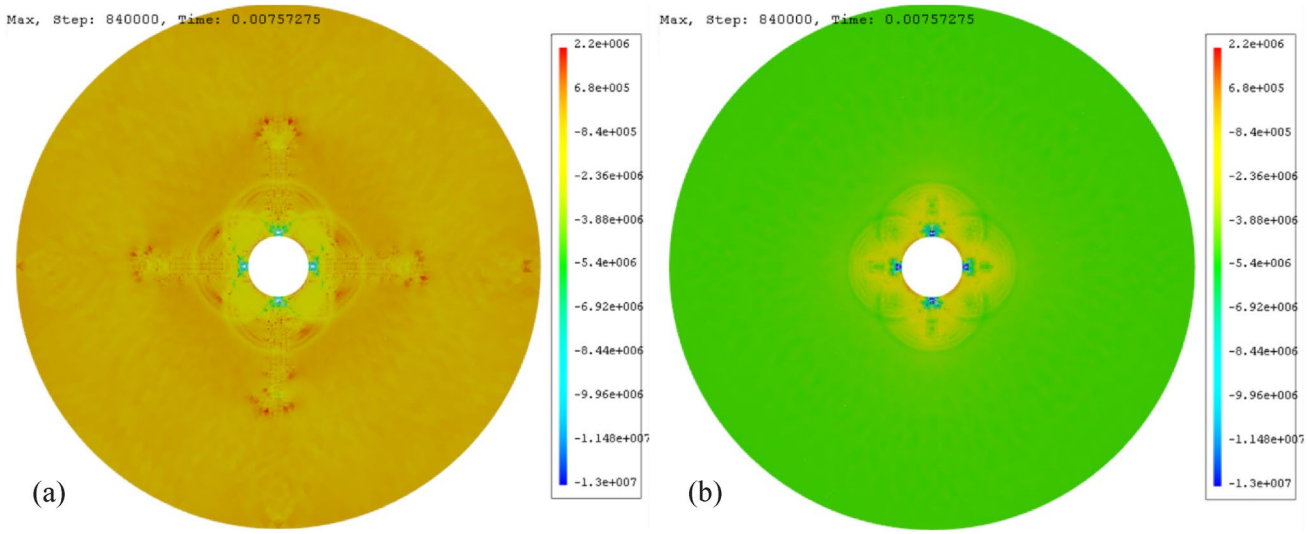

Fig. 4 Maximum principal stress of Rock1 under different tectonic stresses. **a** 1 MPa tectonic stress. **b** 5 MPa tectonic stress

Table 3 Fracture degree under different tectonic stresses

σ_{ini}/MPa	Φ/% (Rock1)	Φ/% (Rock2)	Φ/% (Rock3)
1	12.95	8.05	5.88
3	5.89	3.30	2.53
5	3.95	2.32	1.73

Table 4 Total mass of water injection under different tectonic stresses

σ_{ini}/MPa	M_T/kg (Rock1)	M_T/kg (Rock2)	M_T/kg (Rock3)
1	0.86	0.54	0.46
3	0.65	0.45	0.41
5	0.55	0.42	0.39

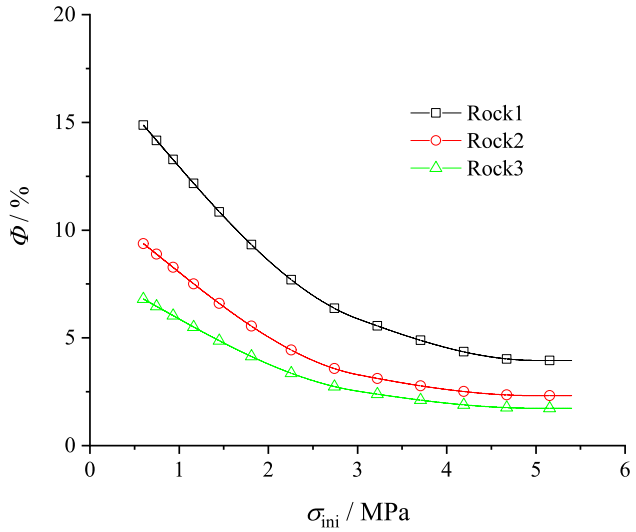

Fig. 5 Fracture degree under different tectonic stresses

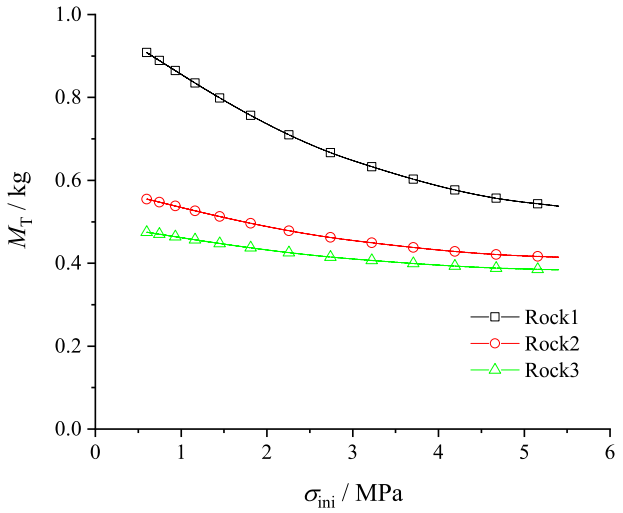

Fig. 6 Total mass of water injection under different tectonic stresses

fractures, the transmission range of fluid pressure along the fracture flow is larger, and the range of tensile stress is larger.

To quantitatively analyze the number of fractures in reservoir under different tectonic stresses, the fracture degree (Φ) of the reservoir is defined as the ratio of the number of crack grids and the total number of grids. After the 10th impact, the fracture degree of different reservoirs under different tectonic stresses (σ_{ini}) is shown in Table 3.

The relationship between fracture degree and tectonic stress after the 10th impact is shown in Fig. 5. The fracture degree decreases nonlinearly with the tectonic stress. When the tectonic stress is low (< 3 MPa), the fracture degree of reservoirs changes more obviously. When the tectonic stress increases to 3 times, the fracture degree of the three reservoirs decrease to approximately 2.3 times. When the tectonic stress increases to 5 times, the fracture degree of the three reservoirs decrease to approximately 3.4 times. The fracture degree does not change in equal proportion with the tectonic stress, and the change rate is 0.77–0.68.

The total mass (M_T) of injected water in three reservoirs under different tectonic stresses are analyzed, which is the mass per unit depth. After the 10th impact, the total mass of injected water in reservoirs under different tectonic stress is shown in Table 4.

The relationship between total mass and tectonic stresses after the 10th impact is shown in Fig. 6. The total mass of injected water decreases nonlinearly with the tectonic stress. The total mass of injected water in Rock 1 is significantly greater than that in Rock 2 and Rock 3. When the tectonic stress increases to 3 times, the total mass of injected water in the reservoir is reduced by 1.32–1.12 times. When the tectonic stress increases to 5 times, the total mass of injected water in the reservoir is reduced by 1.56–1.21 times. The total mass of injected water does not change in equal proportion with the tectonic stress, and the change rate is 0.44–0.24.

Effect of Young's modulus

The rock Young's modulus and Poisson's ratio describe the rock deformation response, which considers significant mechanical properties and can be used to predict the geomechanical behavior during reservoir deformation. Based on the different strengths of Rock1, Rock2, and Rock3, the influence of Young's modulus on reservoir permeability after repeated impact is analyzed. After the 10th impact, the fracture degree of different reservoirs under different Young's modulus (E) is shown in Table 5.

The relationship between fracture degree and Young's modulus after the 10th impact is shown in Fig. 7. The

Table 5 Fracture degree under different Young's modulus

E/GPa	Φ/% (σ_{ini} = 1 MPa)	Φ/% (σ_{ini} = 3 MPa)	Φ/% (σ_{ini} = 5 MPa)
9.13	12.95	5.89	3.95
22.71	8.05	3.30	2.32
36.29	5.88	2.53	1.73

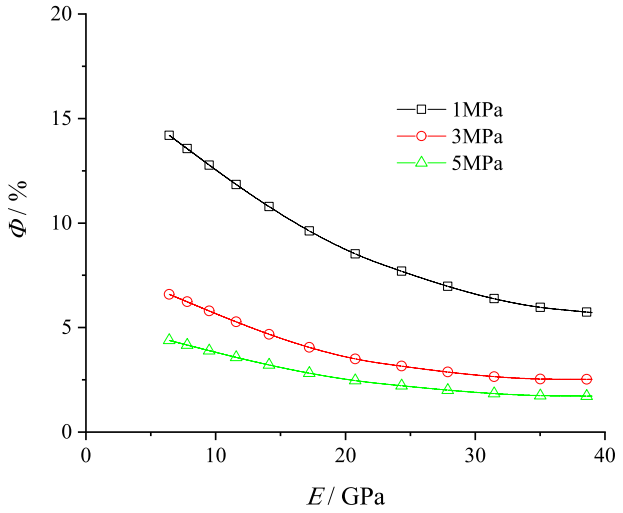

Fig. 7 Fracture degree under different Young's modulus

Table 6 Total mass of water injection under different Young's modulus

σ_{ini}/MPa	M_T/kg (σ_{ini} = 1 MPa)	M_T/kg (σ_{ini} = 3 MPa)	M_T/kg (σ_{ini} = 5 MPa)
9.13	0.86	0.65	0.55
22.71	0.54	0.45	0.42
36.29	0.46	0.41	0.39

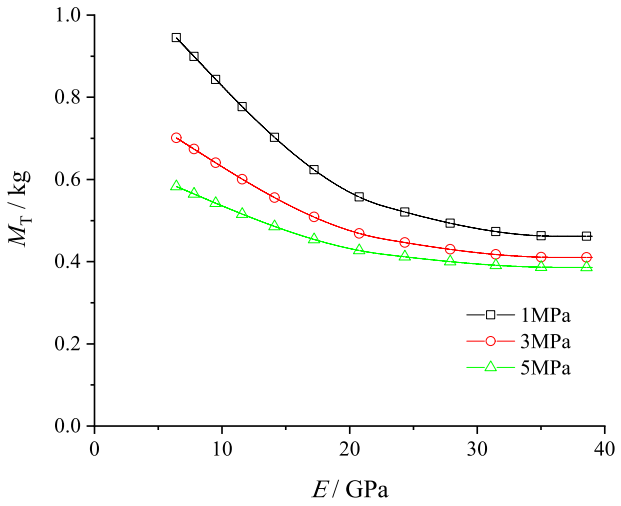

Fig. 8 Total mass of water injection under different Young's modulus

fracture degree of the reservoirs decreases nonlinearly with the Young's modulus. When the Young's modulus is low, the fracture degree of different reservoirs changes more obviously. When the Young's modulus increases to 2.49 times, the fracture degree with different tectonic stresses decreases to approximately 1.7 times. When the Young's modulus increases to 3.97 times, the fracture degree decreases to approximately 2.3 times. The fracture degree does not change in equal proportion with the Young's modulus, and the change rate is 0.68–0.58. Compared with Fig. 5, the effect of tectonic stress on the fracture degree is higher than that of Young's modulus, that is, tectonic stress has greater influence on the number of cracks.

The total mass of injected water in three reservoirs under different Young's modulus is analyzed, which is the mass per unit depth. After the 10th impact, the injected water in different reservoirs under different Young's modulus are shown in Table 6.

The relationship between total mass and Young's modulus after the 10th impact is shown in Fig. 8. The total mass of injected water decreases nonlinearly with the Young's modulus. When the Young's modulus increases to 2.49 times, the total mass of injected water is reduced by 1.6–1.31 times. When the Young's modulus increases to 3.97 times, the total mass of injected water is reduced by 1.85–1.42 times. When the Young's modulus is low, the total mass of injected water changes more obviously. The total mass of injected water does not change in equal proportion with the Young's modulus, and the change rate is 0.64–0.36. Compared with Fig. 6, the effect of Young's modulus on the total mass of injected water is higher than that of tectonic stress. It can be inferred that Young's modulus has an effect on the space of the reservoir after fracturing, that is, it has a great effect on the fracture aperture. Therefore, the number of fractures is more sensitive to tectonic stress, and the fracture aperture is more sensitive to Young's modulus of elasticity. The number of fractures and the fracture aperture jointly affect the permeability of the reservoir. When the reservoir strength and tectonic stress are relatively low, the permeability of the reservoir is easier to increase.

Effect of repeated impact

CWS is the power source of reservoir fracturing, and the number of shocks can effectively change the permeability of the reservoir. Under repeated impact, the influence of impact times on reservoir permeability is analyzed. When the tectonic stress is 1 MPa, the maximum principal stress of Rock1 during the 2th, 4th, 6th and 8th impact are shown

in Fig. 9. The stress wave of CWS is transmitted to the reservoir along the perforation. With the increase of impact times, the number and length of reservoir fractures gradually increase. The maximum length of fractures is 0.45 m, 0.55 m, 0.65 m and 0.75 m respectively, which almost linearly increases with the impact times. Along the increase in the number and length of fractures, the range of tensile stress at the front of the fracture also gradually increases. The reservoir around the wellbore forms three zones, which can be regarded as the compression zone, tension zone and undamaged zone from near to far. When the repeated impact is less, the main fracture along the perforation direction is formed. When repeated impact increases, the main fracture length increases, and a large number of fractures in different directions will appear around the main fracture, forming a complex fracture network. The repeated impact of CWS can make the existing fractures longer and wider and can also make the new fractures more widely distributed so that the fractures show a more obvious spider-web structure, which may be beneficial to the improvement of reservoir permeability.

The low (1 MPa) and high (5 MPa) tectonic stresses are selected to analyze the fracture degree after multiple impacts. The fracture degree of different reservoirs after 1th impact is shown in Table 7, the fracture degree of different reservoirs after 10th impact is shown in Table 8.

The relationship between fracture degree and impact times (T) is shown in Fig. 10. When the tectonic stress is low (Fig. 10a), the fracture degree of the three reservoirs increases with repeated impact, showing an obvious step shape. For different reservoirs, the fracture degree increases to 1.7 times in almost all reservoirs after 10th impact. When the tectonic stress is high (Fig. 10b), the fracture degree of different reservoirs increases differently under repeated

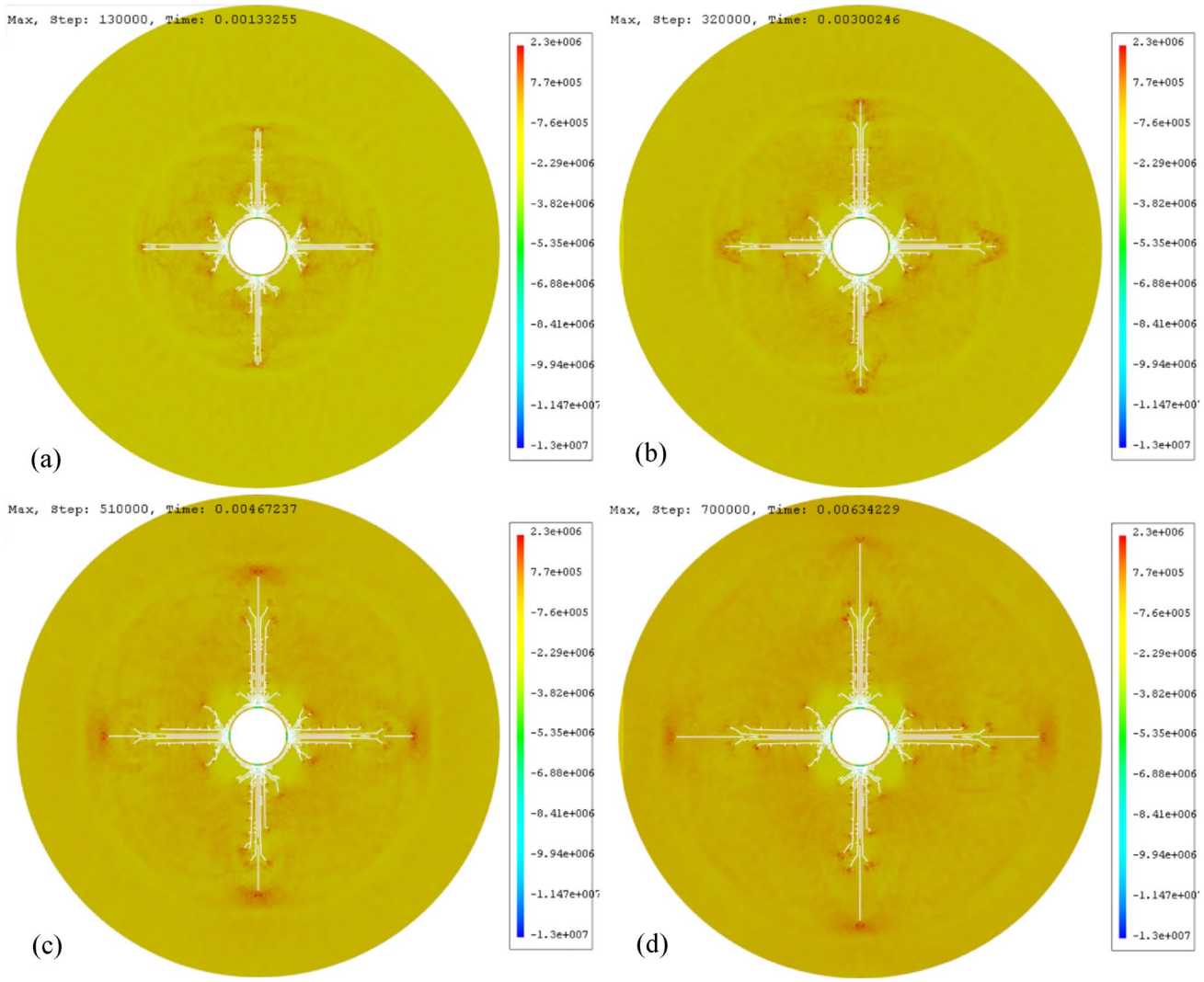

Fig. 9 Maximum principal stress of Rock1 under repeated impact. **a** 2th impact. **b** 4th impact. **c** 6th impact. **d** 8th impact

Table 7 Fracture degree under 1 MPa tectonic stress

	Φ/% (1th impact)	Φ/% (10th impact)
Rock1	7.18	12.95
Rock2	5.07	8.05
Rock3	3.38	5.88

Table 8 Fracture degree under 5 MPa tectonic stress

	Φ/% (1th impact)	Φ/% (10th impact)
Rock1	2.27	3.95
Rock2	1.66	2.32
Rock3	1.26	1.73

The relationship between the total mass of water injection and repeated impact is shown in Fig. 11. When the tectonic stress is low (Fig. 11a), the total mass of water injection in the three reservoirs increases with repeated impact, showing an obvious step shape. After the 10th impact, the total mass of water injection in three reservoirs increased by 2.1 times, 1.5 times and 1.3 times respectively. When the tectonic stress is high (Fig. 11b), the total mass of water injection in reservoirs increases differently under repeated impact, and Rock1 is greater than Rock2 and Rock3.For the three reservoirs, the total mass of water injection increases by approximately 1.4, 1.1 and 1.1 times, respectively. Under different tectonic stresses, the trend of repeated shock to improve the total mass of water injection is similar, which indicates that multiple shock waves can effectively increase fracture aperture. In addition, when the tectonic stress is large, the total mass of water injection is close to linear with the number

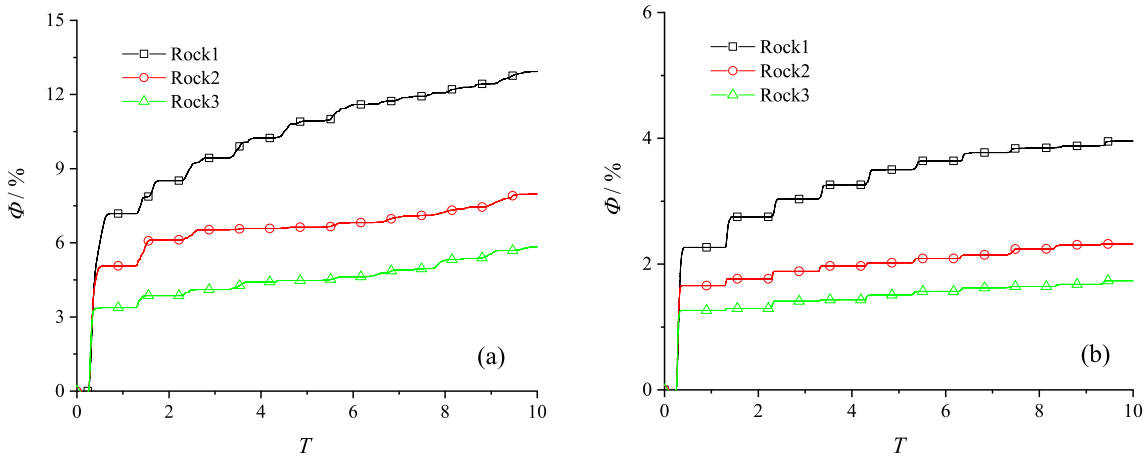

Fig. 10 Fracture degree under different repeated impact. **a** 1 MPa tectonic stress. **b** 5 MPa tectonic stress

Table 9 Total mass of water injection under 1 MPa tectonic stress

	M_T/ kg (1th impact)	M_T/kg (10th impact)
Rock1	0.41	0.86
Rock2	0.37	0.54
Rock3	0.36	0.46

Table 10 Total mass of water injection under 5 MPa tectonic stress

	M_T/ kg (1th impact)	M_T/kg (10th impact)
Rock1	0.39	0.55
Rock2	0.37	0.42
Rock3	0.36	0.39

impact, and Rock1 is greater than Rock2 and Rock3. For the three reservoirs, the fracture degree increases by approximately 1.7, 1.4 and 1.4 times, respectively. Under different tectonic stresses, the trend of repeated shock to improve the fracture degree is similar, which indicates that multiple shock waves can effectively increase the number of fractures.

The total mass of water injection in reservoirs after 1th impact is shown in Table 9, the total mass of water injection in reservoirs after 10th impact is shown in Table 10.

of shocks, but the increment is not obvious, which may be related to the initial energy of the shock wave. The initial energy of CWS can be controlled efficiently, and improving the initial energy can also improve the mass of water injection, thus improving the permeability of the reservoir.

Through the relationship between water injection time and water injection flow, it can be found that the reservoir permeability has been improved. Under different tectonic

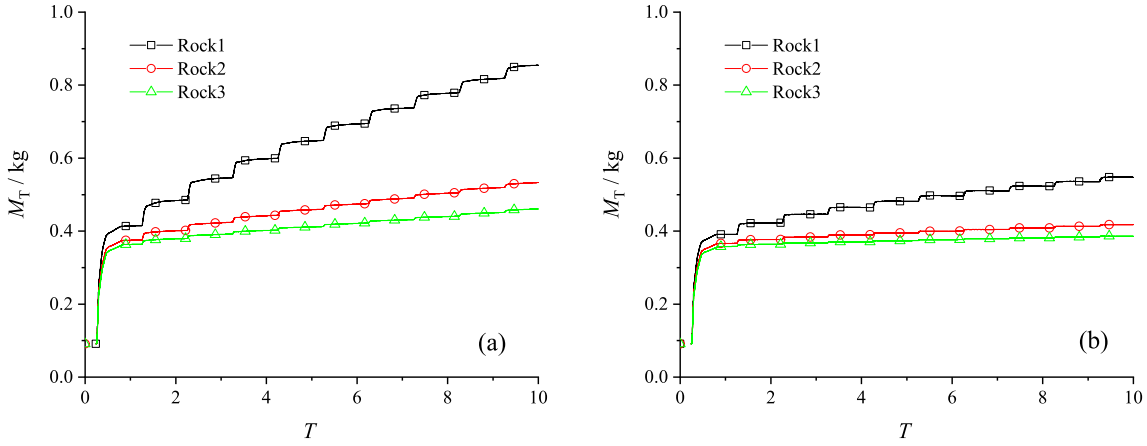

Fig. 11 Total mass of water injection under different repeated impact. **a** 1 MPa tectonic stress. **b** 5 MPa tectonic stress

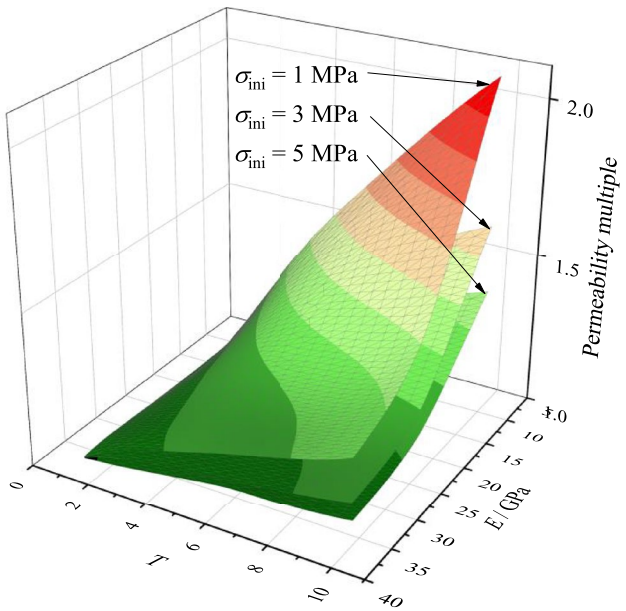

Fig. 12 Relationship between repeated impact, reservoir strength and permeability multiple under different tectonic stresses

stress and different reservoir strength, the value of reservoir permeability is significantly different. Therefore, it is not of general significance to only discuss the value of permeability under repeated impact. Compared with the first impact, the increase rate of reservoir permeability after repeated impact is analyzed, as shown in Fig. 12. For reservoirs with low tectonic stress and strength, repeated impact significantly improves the reservoir permeability, but for reservoirs with high tectonic stress and strength, the permeability enhancement is not obvious. The permeability of reservoirs with different tectonic stresses and strengths increases nonlinearly and monotonicly with repeated impact. This nonlinear and monotonic three-dimensional relationship has considerable practical significance in engineering. For reservoirs with different tectonic stress and strength in engineering practice, the change of reservoir permeability can be predicted by controlling the parameters of CWS (peak pressure, duration, impact times, etc.) through the above three-dimensional relationship. Therefore, the reservoir fracturing scheme can be optimized, and the reservoir fracturing efficiency can be improved.

Conclusions

Based on the continuous-discontinuous element method (CDEM), the coupling mechanism of deformation, failure, pore seepage, and fracture flow is considered, and a multiphysical field coupling model for reservoir permeability enhancement under controllable shock wave (CWS) is proposed. The dynamic process of formation and development of reservoir fractures is obtained under fluid–solid coupling conditions, and the change of reservoir permeability is obtained under the action of multiple factors. The main conclusions were the following:

1. The stress wave generated by CWS is transmitted to the reservoir along the perforation. Under repeated impact, fractures are generated near the wellbore by compression, and more fractures are generated in front of existing fractures by tension. After repeated impact, the length of the main fracture increases, and a large number of fractures in different directions will appear around the main fracture, forming a complex fracture network, which is different from traditional hydraulic fracturing. The repeated impact of CWS can make the existing fractures longer and wider, and also make the new fractures more widely distributed, so that the frac-

tures show a more obvious spider web structure, which may be beneficial to improve the reservoir permeability.
2. After repeated impact, the number of fractures affected by tectonic stress is 1.13 times greater than that of reservoir strength, the number of fractures is more sensitive to tectonic stress. The total mass of injected water affected by reservoir strength is 1.5 times greater than that of tectonic stress, the fracture aperture is more sensitive to reservoir strength.
3. The permeability of reservoirs with different tectonic stresses and strengths increases nonlinearly and monotonicly with repeated impacts. The coupling model based on CDEM can efficiently obtain that complex three-dimensional relationship. Through that relationship, for reservoirs with different tectonic stress and strength, CWS parameters can be controlled to predict the change of reservoir permeability, such as peak pressure, duration, impact times, etc. Therefore, that method can optimize the reservoir fracturing scheme and improve the reservoir fracturing efficiency, which has considerable practical significance.

Funding This work was funded by the National Natural Science Foundation of China (NO. 11802312 and NO. U1762216) and by the National Science and Technology Major Project of the Ministry of Science and Technology of China Project (NO. 2016ZX05037006). Xinguang Zhu, Chun Feng and Pengda Cheng declared that the funds had received support from the National Natural Science Foundation of China (NO. 11802312 and NO. U1762216) and the National Science and Technology Major Project of the Ministry of Science and Technology of China Project (NO. 2016ZX05037006). The funders had no role in study design, data collection and analysis, decision to publish, or preparation of the manuscript.

Declarations

Conflict of interest The authors declare that they have no known competing financial interests or personal relationships that could have appeared to influence the work reported in this paper.

References

Azad M, Ghaedi M, Farasat A, Parvizi H, Aghaei H (2022) Case study of hydraulic fracturing in an offshore carbonate oil reservoir. Pet Res 7(4):419–429. https://doi.org/10.1016/j.ptlrs.2021.12.009

Chen B, Barboza BR, Sun Y, Bai J, Thomas HR, Dutko M, Cottrell M, Li C (2022) A review of hydraulic fracturing simulation. Arch Comput Methods Eng 29(4):1–58. https://doi.org/10.1007/s11831-021-09653-z

Cheng AH-D (2016) Poroelasticity, vol 27. Springer International Publishing, Berlin. https://doi.org/10.1007/978-3-319-25202-5

Cheng P, Shen W, Xu Q, Lu X, Qian C, Cui Y (2022) Multiphysics coupling study of near-wellbore and reservoir models in ultra-deep natural gas reservoirs. J Pet Explor Prod Technol 12(8):2203–2212. https://doi.org/10.1007/s13202-021-01424-7

Dontsov EV, Peirce AP (2017) A multiscale Implicit Level Set Algorithm (ILSA) to model hydraulic fracture propagation incorporating combined viscous, toughness, and leak-off asymptotics. Comput Methods Appl Mech Eng 313:53–84. https://doi.org/10.1016/j.cma.2016.09.017

Dontsov EV, Zhang F (2018) Calibration of tensile strength to model fracture toughness with distinct element method. Int J Solids Struct 144–145:180–191. https://doi.org/10.1016/j.ijsolstr.2018.05.001

Esfandiari M, Pak A (2023) XFEM modeling of the effect of in-situ stresses on hydraulic fracture characteristics and comparison with KGD and PKN models. J Pet Explor Prod Technol 13(1):185–201. https://doi.org/10.1007/s13202-022-01545-7

Feng C, Liu X, Lin Q, Li S (2022) A simple particle–spring method for capturing the continuous–discontinuous processes of brittle materials. Eng Anal Bound Elem 139:221–231. https://doi.org/10.1016/j.enganabound.2022.03.015

Gong D, Chen J, Wang W, Qu G, Zhu J, Wang X, Zhang H (2022) Numerical simulations of radial well assisted deflagration fracturing based on the smoothed particle hydrodynamics method. Processes 10(12):2535. https://doi.org/10.3390/pr10122535

Lecampion B, Bunger A, Zhang X (2018) Numerical methods for hydraulic fracture propagation: a review of recent trends. J Nat Gas Sci Eng 49:66–83. https://doi.org/10.1016/j.jngse.2017.10.012

Li X, Xiao W, Qu Z, Guo T, Li J, Zhang W, Tian Y (2018) Rules of fracture propagation of hydraulic fracturing in radial well based on XFEM. J Pet Explor Prod Technol 8(4):1547–1557. https://doi.org/10.1007/s13202-018-0436-5

Li J, Feng C, Zhu X, Zhang Y (2022) Analysis of the coal fluidization mining process with the continuous-discontinuous coupled particle-block method. Geofluids 2022:1–11. https://doi.org/10.1155/2022/7001654

Ma T, Zhang K, Shen W, Guo C, Xu H (2021) Discontinuous and continuous Galerkin methods for compressible single-phase and two-phase flow in fractured porous media. Adv Water Resour 156:104039. https://doi.org/10.1016/j.advwatres.2021.104039

Maulianda B, Savitri CD, Prakasan A, Atdayev E, Yan TW, Yong YK, Elrais KA, Barati R (2020) Recent comprehensive review for extended finite element method (XFEM) based on hydraulic fracturing models for unconventional hydrocarbon reservoirs. J Pet Explor Prod Technol 10(8):3319–3331. https://doi.org/10.1007/s13202-020-00919-z

Parvizi H, Rezaei-Gomari S, Nabhani F (2017) Robust and flexible hydrocarbon production forecasting considering the heterogeneity impact for hydraulically fractured wells. Energy Fuels 31(8):8481–8488. https://doi.org/10.1021/acs.energyfuels.7b00738

Peirce AP, Siebrits E (2001) Uniform asymptotic approximations for accurate modeling of cracks in layered elastic media. Int J Fract 110(3):205–239. https://doi.org/10.1023/A:1010861821959

Prasad Singh SS, Agarwal JR, Mani N (2019) Offshore drilling and completion. Offshore Operations and Engineering. CRC Press, Boca Raton, pp 43–97. https://doi.org/10.1201/9780429354533-3

Qin Y, Li H, Zhang Y, Zhao Y, Zhao J, Qiu A (2021) Numerical analysis on CSW fracturing behavior of coal seam under constraint of geological and engineering conditions. Coal Geol Explor 49(1):108–118

Shen W, Ma T, Li X, Sun B, Hu Y, Xu J (2022) Fully coupled modeling of two-phase fluid flow and geomechanics in ultra-deep natural gas reservoirs. Phys Fluids 34(4):043101. https://doi.org/10.1063/5.0084975

Shi S, Shi C, Tian G, Lin B, Yu H, Wei S, Wang Z (2023) Stress evolution and fracture propagation of infill well after production and injection of parent well in a tight oil reservoir. J Pet Explor Prod Technol. https://doi.org/10.1007/s13202-022-01605-y

Tan P, Jin Y, Han K, Hou B, Chen M, Guo X, Gao J (2017) Analysis of hydraulic fracture initiation and vertical propagation behavior in laminated shale formation. Fuel 206:482–493. https://doi.org/10.1016/j.fuel.2017.05.033

Wang J, Xue Q, Du X, Cao Y, Yu J, Zhou P, Jiang H (2021) Study on the unplugging technology through electric explosion controllable shock wave. J Energy Resour Technol. https://doi.org/10.1115/1.4049584

Wang H, Yu A, Feng C, Ling X, Chen G, Gu M, Zhu X (2022) An Efficient CDEM-based method to calculate full time-space natural fragment field of shell-bearing explosives. Int J Impact Eng 161:104099. https://doi.org/10.1016/j.ijimpeng.2021.104099

Wu F, Wei X, Chen Z, Rahman SS, Pu C, Li X, Zhang Y (2018a) Numerical simulation and parametric analysis for designing high energy gas fracturing. J Nat Gas Sci Eng 53:218–236. https://doi.org/10.1016/j.jngse.2018.02.011

Wu J, Yin G, Fan Y, Li X, Qiu A (2018b) Review of electrical exploding wires-(II):underwater. High Volt Eng 44(12):4003–4012

Yang Y, Tang X, Zheng H, Liu Q, Liu Z (2018) Hydraulic fracturing modeling using the enriched numerical manifold method. Appl Math Model 53:462–486. https://doi.org/10.1016/j.apm.2017.09.024

Yang W, Zheng C, Li A, Yin S, Guo X, Zhao Z, Lu Y (2020) Feasibility analysis of controllable shock wave induced cracking in offshore oil reservoir. Drill Prod Technol 43(1):38–41

Yu S, Ting L, Meng W, Xiaoqi W, Fangkai Q, Cheng Z (2022) Desorption of CH4/CO2 from kerogen during explosive fracturing. Fuel 324:124741. https://doi.org/10.1016/j.fuel.2022.124741

Yue Z, Zhou J, Feng C, Li A, Qiu P, Gang M (2021) Numerical investigation of the effect of holes on dynamic fracturing in multi-flawed granite. Fatigue Fract Eng Mater Struct 44(7):1883–1896. https://doi.org/10.1111/ffe.13474

Zhang Y, Qiu A, Zhou H, Liu Q, Tang J, Liu M (2016) Research progress in electrical explosion shockwave technology for developing fossil energy. High Volt Eng 42(4):1009–1017

Zhang Y, Gao Z, Li Y, Zhuang X (2020) On the crack opening and energy dissipation in a continuum based disconnected crack model. Finite Elem Anal Des 170:103333. https://doi.org/10.1016/j.finel.2019.103333

Zhu X, Feng C, Cheng P, Wang X, Li S (2021) A novel three-dimensional hydraulic fracturing model based on continuum–discontinuum element method. Comput Methods Appl Mech Eng 383:113887. https://doi.org/10.1016/j.cma.2021.113887